The 16th International Congress on the Chemistry of Cement 2023 (ICCC2023)
"Further Reduction of CO_2 -Emissions and Circularity in the Cement and Concrete Industry"
September 18–22, 2023, Bangkok, Thailand

Impact of autoclaving on the phase assemblage of Portland cement: Experiment and thermodynamic modelling

T. Hirsch[1,*], M. Voigt[2], C. Lehmann[1], B. Meng[2], and B. Lothenbach[3,4]

[1] *Technische Universität Berlin, Faculty VI Planning Building Environment, Building Materials and Construction Chemistry, Berlin, Germany*
Email: t.hirsch@tu-berlin.de, c.lehmann@tu-berlin.de

[2] *Bundesanstalt für Materialforschung und -prüfung, Fachbereich 7.1 Baustoffe, Berlin, Germany*
Email: marieke.voigt@bam.de, birgit.meng@bam.de

[3] *Empa, Concrete & Asphalt Laboratory, Dübendorf, Switzerland*
[4] *NTNU, Department of Structural Engineering, Trondheim, Norway*
Email: barbara.lothenbach@empa.ch

ABSTRACT

Even after autoclaving for 2 weeks in the temperature range of 120 to 200 °C, CEM I paste with a water-to-cement ratio of 0.5 still contains some low-crystalline C-S-H. The conversion of low-crystalline C-S-H to crystalline is faster with increasing temperature. The observed low-crystalline and crystalline C-S-H phases (reinhardbraunsite, jaffeite) indicate that the samples have not reached equilibrium yet under these experimental conditions. However, there is a good agreement between experiment and thermodynamic modelling for the other solids indicating that the used datasets are suitable for this application.

KEYWORDS: *Autoclaving, Crystalline C-S-H, Scawtite, Hydroxylellestadite*

1. Introduction

When concrete is exposed to hydrothermal conditions beyond 100 °C, the phase assemblage changes substantially (Werder et al. 2021; Tian et al. 2022). Such conditions are typically applied in the production of autoclaved (aerated) concrete, calcium silicate bricks and other autoclaved calcium silicate building products (Society of Chemical Industry 1967; Kikuma et al. 2009). The low-crystalline C-S-H gel observed at room temperature is replaced by crystalline C-S-H phases. Sulfate is bound in calcium sulfates or hydroxylellestadite. Depending upon the system chemistry, portlandite and hydrogarnet may occur.
Thermodynamic modelling is frequently performed for temperatures below 100 °C and has strongly enhanced the understanding of cement hydration and deterioration (Lothenbach and Zajac 2019). Beyond 100 °C, however, thermodynamic data for hydrated cements is lacking. The current publication compares experimental observations for a CEM I paste with predictions made by the combination of thermodynamic datasets commonly used in cement science with the recent dataset of Hirsch et al..

2. Materials and methods

The oxide composition of the CEM I 52.5 R (Dyckerhoff) used was determined by X-ray fluorescence (XRF) using a WD-RFA PW 2400 (Philips) based on powder tablets as well as fused discs. Water and carbon dioxide were quantified by thermogravimetric analysis (TG) using a TG2 09 F3 Tarsus (Netzsch) heating at 10 °C/min from room temperature to 850 °C in a nitrogen atmosphere with a flow rate of 40 mL/min. The results are presented in Table 1.

Table 1: Oxide composition of used CEM I as determined by XRF and TG.

Al_2O_3	CaO	Fe_2O_3	K_2O	MgO	MnO	Na_2O	P_2O_5	SiO_2	SO_3	TiO_2	CO_2	H_2O	Sum
3.64	66.24	1.44	0.6	0.91	0.04	0.3	0.16	21.78	2.72	0.21	1.57	0.86	100.47

Cement paste was prepared at a water-to-cement ratio of 0.5 using a planetary centrifugal mixer. The paste was filled in cylindrical molds of 22.6 by 22.6 mm, covered with foil, and stored at 23 °C and 50% relative humidity for 24 h. After demolding, the samples were autoclaved at the target temperatures (120 to 200 °C in 20 K increments) for 14 days under saturated water vapor pressure and, after this, cooled in the autoclave to room temperature. Subsequently, the samples were crushed, ground with isopropanol in a McCrone mill and dried under vacuum at 40 °C for 2 days. The powder samples were mixed with an internal standard (10 wt% of ZnO). X-ray diffraction was performed with a Bragg-Brentano diffractometer (Empyrean, PANalytical). The Cu Kα radiation was generated with 40 kV and 40 mA, filtered by Ni and measured by a PiXcel^{1D}. For phase quantification, Rietveld refinements were performed using HighScore Plus 4.8. The structure data used for the refinements was taken from ICSD and is listed in Table 2.

Table 2: Phases with ICSD structure numbers used for Rietveld refinements.

Alite	22501	Portlandite	73467
Tricalcium aluminate	1880	Hydroxylellestadite	39775
Hydrogarnet (larger unit cell)	49772	Jaffeite	39725
Hydrogarnet (smaller unit cell)	172076	Reinhardbraunsite	200924
Calcite	166364	ZnO	155780

The thermodynamic modelling was conducted using the thermodynamic software GEMS (Kulik et al. 2012; Wagner et al. 2012) version 3.7. The databases PSI/Nagra 12/07 (Thoenen and Kulik 2003; Thoenen et al. 2014), Cemdata18 (Lothenbach et al. 2019) and datasets for zeolites (Ma and Lothenbach 2020a, 2020b) provided basic thermodynamic properties. Furthermore, the database cCSH for crystalline C-S-H and some additional phases forming at elevated temperatures and pressures (Hirsch et al.) was included. As the datasets of Ma and Lothenbach contain data for zeolites, the zeolites of Cemdata18 were deactivated for internal consistency. The species $Si_4O_8(OH)_4^{4-}$ of PSI/Nagra was deactivated as its data are only reliable for ambient conditions.

3. Results

The experimental results are presented in Figure 1. Despite a dwell time of 2 weeks, the samples autoclaved at 120 to 160 °C still contain small quantities of clinker phases, which diminish with rising temperature.

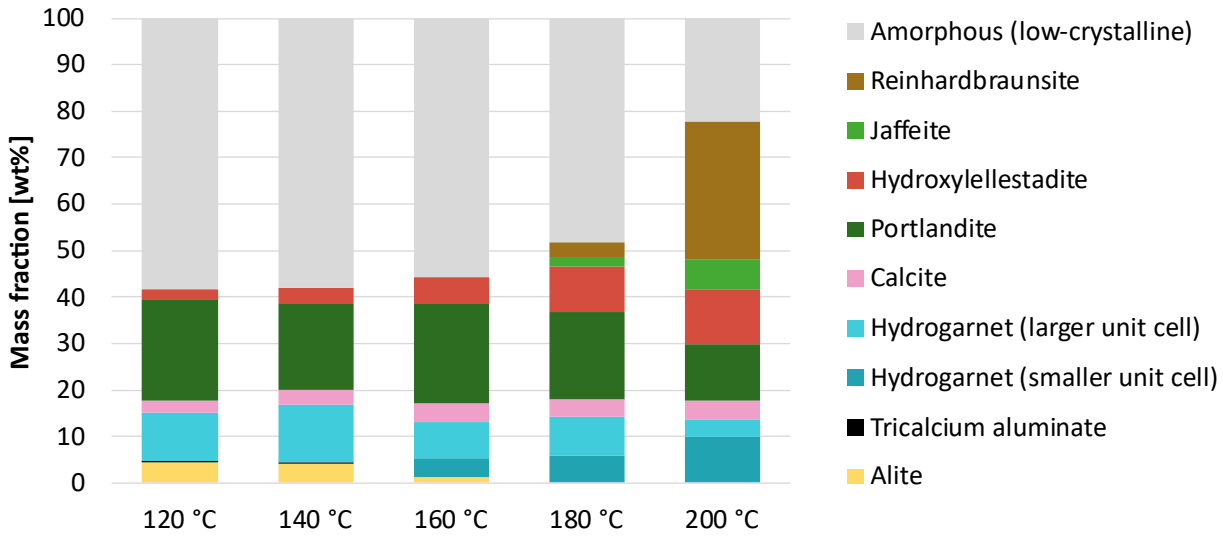

Figure 1: Solid phase assemblage in autoclaved pastes as determined by Rietveld refinement.

In general, the samples are quite similar in their phase assemblage. Nevertheless, a splitting of the hydrogarnet reflexes in XRD occurs in the temperature range between 140 and 160 °C, which persists at higher temperature. The summed share of the two hydrogarnets varies however only slightly between all samples. The share of calcite is nearly constant and increases only very slighty between 120 and 160 °C.

Further phases present in all samples are a low-crystalline phase (very likely C-S-H), portlandite and hydroxylellestadite. At lower temperatures, the low-crystalline C-S-H accounts for more than half of the sample. In the samples autoclaved at 180 and 200 °C, the two crystalline C-S-H phases reinhardbraunsite and jaffeite appear. While their share is still small at 180 °C, both, in particular reinhardbraunsite, gain at 200 °C while the portion of low-crystalline C-S-H diminishes. Simultaneously, a strong increase in the quantities of hydroxylellestadite and decrease of portlandite can be observed. Both of these effects are likely due to the reaction of low-crystalline C-S-H, which liberates the sulfate adsorbed on its large surface (Barbarulo et al. 2007). The destabilization of low-crystalline C-S-H leads consequently to release of sulfate, which is bound in hydroxylellestadite. Portlandite is likely consumed as the formation of reinhardbraunsite and jaffeite from low-crystalline C-S-H requires additional Ca.
Thermodynamic modelling predicts the formation of hillebrandite in the whole temperature range and meta-ettringite around 200 °C. Ettringites are known to be low temperature phases (Zhou and Glasser 2001), indicating an overestimation of the metaettringite stability at 200°C. Hillebrandite was not observed in the current experiments, and is known to form very slow or not at all depending on the experimental conditions (Garbev 2004). Consequently, both phases were deactivated in the modelling. The resulting thermodynamic models are qualitatively quite close to the experiment (Figure 2). The existence of portlandite, hydrogarnet, hydroxylellestadite and a small quantity of calcite agrees well with the experimental observations. The modelling even predicts the formation of two individual hydrogarnets indicating that the persistence of one sole hydrogarnet in the low-temperature samples may be due to kinetic reasons. Hydrotalcite and pyrolusite are predicted as well but not observed experimentally, which might be due to their small quantities and potentially low crystallinity (pyrolusite is not visible in Figure 2 due to low quantity). In experiment and simulation, the phase assemblage is dominated by C-S-H phases. The low-crystalline C-S-H in the experiment is likely metastable as:

- Experiments in the literature show that increase in dwell time and water content yield in more crystalline C-S-H phases
- Thermodynamic modelling predicts crystalline C-S-H (Figure 2)
- At higher temperature, the low-crystalline C-S-H decreases in quantity and crystalline C-S-H phases form, which occur in the thermodynamic predictions (Figure 1)

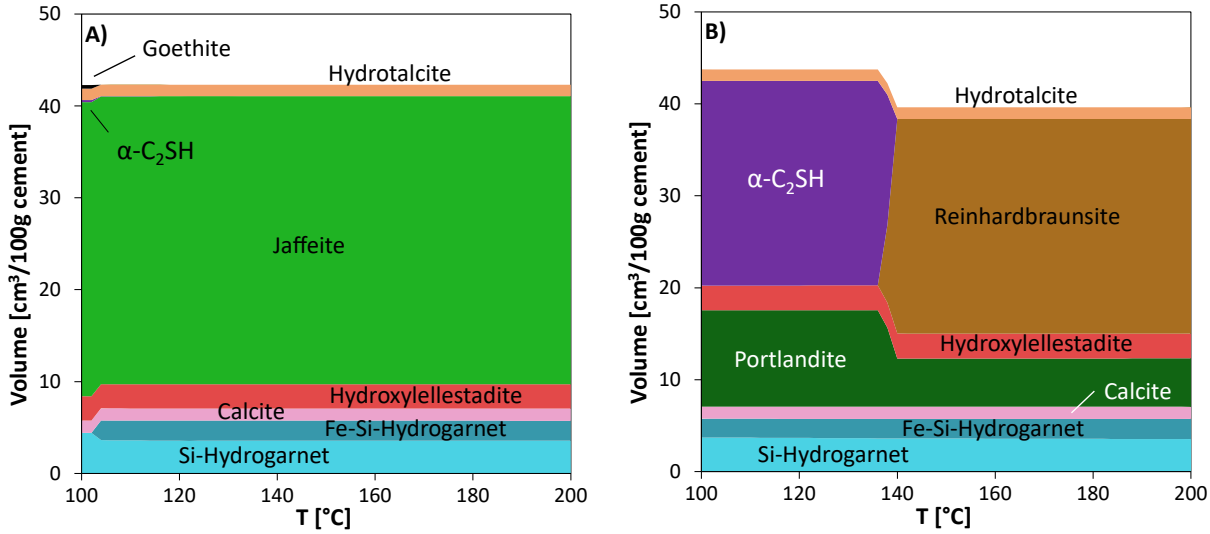

Figure 2: Thermodynamic modelling of the phase assemblage in autoclaved CEM I paste. A) with suppressed formation of metaettrinigte and hillebrandite, B) with suppressed formation of metaettrinigte, hillebrandite and jaffeite.

Hillebrandite formation seems to be kinetically hindered in the experiments. If hillebrandite is suppressed in the modelling, the formation of jaffeite is predicted but not of reinhardbraunsite. Reinhardbraunsite is only predicted if also jaffeite is prohibited to form. The samples at higher temperature possess higher shares of reinhardbraunsite than jaffeite. This could be interpreted in the way that reinhardbraunsite forms faster

than jaffeite (and hillebrandite) under the experimental conditions, potentially because less portlandite is required for the reaction of low-crystalline C-S-H to reinhardbraunsite than is needed for the reaction to jaffeite.

4. Conclusions

Combining several thermodynamic databases, the experimentally observed phase assemblage of a CEM I paste exposed to autoclaving was modelled successfully. Experimental results and modelling indicate that the C-S-H phases are still far from equilibrium after 2 weeks. Crystalline C-S-H phases were not observed in samples autoclaved between 120 and 160 °C. The other phases are found in the experiment as predicted by thermodynamic modelling disregarding minor phases. Further comparison studies between experimental work and thermodynamically predicted phase assemblages should be untertaken to test and refine the datasets.

Acknowledgements

The authors are grateful for founding of this work by German Federal Ministry of Economic Affairs and Energy in scope of the project “BeHeWaDS” (03ET1537A).

References

Barbarulo, R.; Peycelon, H.; Leclercq, S. (2007): Chemical equilibria between C–S–H and ettringite, at 20 and 85 °C. In *Cem. Concr. Res.* 37 (8), pp. 1176–1181. DOI: 10.1016/j.cemconres.2007.04.013.

Garbev, K. (2004): Struktur, Eigenschaften und quantitative Rietveldanalyse von hydrothermal kristallisierten Calciumsilikathydraten (C-S-H-Phasen). Forschungszentrum Karlsruhe in der Helmholtz-Gemeinschaft, Wissenschaftliche Berichte FZKA 6877. Doctoral thesis. Ruprecht-Karls-Universität Heidelberg, Heidelberg. Institut für Technische Chemie.

Hirsch, T.; Lothenbach, B.: Phase stabilities and thermodynamic properties of crystalline $CaO–SiO_2–H_2O$ phases above 100 °C (to be submitted).

Kulik, D.A.; Wagner, T.; Dmytrieva, S.V.; Kosakowski, G.; Hingerl, F.F.; Chudnenko, K.V.; Berner, U.R. (2012): GEM-Selektor geochemical modeling package: revised algorithm and GEMS3K numerical kernel for coupled simulation codes. In *Comput. Geosci.* 26 (012025), p. 189. DOI: 10.1007/s10596-012-9310-6.

Lothenbach, B.; Kulik, D.A.; Matschei, T.; Balonis, M.; Baquerizo, L.; Dilnesa, B. et al. (2019): Cemdata18: A chemical thermodynamic database for hydrated Portland cements and alkali-activated materials. In *Cem. Concr. Res.* 115, pp. 472–506. DOI: 10.1016/j.cemconres.2018.04.018.

Lothenbach, B.; Zajac, M. (2019): Application of thermodynamic modelling to hydrated cements. In *Cem. Concr. Res.* 123, p. 105779. DOI: 10.1016/j.cemconres.2019.105779.

Ma, B.; Lothenbach, B. (2020a): Synthesis, characterization, and thermodynamic study of selected Na-based zeolites. In *Cem. Concr. Res.* 135, p. 106111. DOI: 10.1016/j.cemconres.2020.106111.

Ma, B.; Lothenbach, B. (2020b): Thermodynamic study of cement/rock interactions using experimentally generated solubility data of zeolites. In *Cem. Concr. Res.* 135, p. 106149. DOI: 10.1016/j.cemconres.2020.106149.

Thoenen, T.; Hummel, W.; Berner, U.; Curti, E. (2014): The PSI/Nagra Chemical Thermodynamic Database 12/07. PSI report 14-04. Edited by Nuclear Energy and Safety Research Department Laboratory for Waste Management (LES). Paul Scherrer Institut (PSI). Villigen, Switzerland.

Thoenen, T.; Kulik, D. (2003): Nagra/PSI Chemical Thermodynamic Data Base 01/01 for the GEM-Selektor (V.2-PSI) Geochemical Modeling Code: Release 28-02-03. Internal Report TM-44-03-04. Edited by Paul Scherrer Institut (PSI). Available online at http://gems.web.psi.ch/TDB/doc/pdf/TM-44-03-04-web.pdf.

Tian, H.; Hirsch, T.; Stephan, D.; Lehmann, C. (2022): The Influence of Long-Term Autoclaving on the Properties of Ultra-High Performance Concrete. In *Front. Mater.* 9, Article 844268, p. 38. DOI: 10.3389/fmats.2022.844268.

Wagner, T.; Kulik, D.A.; Hingerl, F.F.; Dmytrieva, S.V. (2012): GEM-Selektor geochemical modeling package: TSolMod library and data interface for multicomponent phase models. In *Can. Mineral.* 50 (5), pp. 1173–1195. DOI: 10.3749/canmin.50.5.1173.

Werder, J. von; Simon, S.; Gardei, A.; Fontana, P.; Meng, B. (2021): Thermal and hydrothermal treatment of UHPC: influence of the process parameters on the phase composition of ultra-high performance concrete. In *Mater Struct* 54 (1), p. 250. DOI: 10.1617/s11527-021-01633-w.

Zhou, Q.; Glasser, F.P. (2001): Thermal stability and decomposition mechanisms of ettringite at <120°C. In *Cem. Concr. Res.* 31 (9), pp. 1333–1339. DOI: 10.1016/S0008-8846(01)00558-0.